Vol.2, No.5, Page 432- 439, 2024 https://doi.org/10.59628/jast.v2i5.1274 ISSN 2958-9568 JAST

SUN PUBLISHER

مجلة جامعة صنعاء للعلوم التطبيقية والتكنولوجيا
Sana'a University Journal of Applied Sciences and Technology
https://journals.su.edu.ye/index.php/jast/

Influence of astigmatic aberration on partially coherent Gaussian-Schell vortex beam focused by lensacon

H. O. Al-Nadary [1,4], Shukri A. M. Kaid [2,1], Abdu A. Alkelly [1], Hassan T. Al-Ahsab [3] and M. S. Qusaila [1]

[1]**Department of Physics, Faculty of Science, University of Sana'a, Sana'a, Yemen,**
[2]**Department of Physics, Faculty of Sci, University of Taiz , Taiz, Yemen,**
[3]**Department of Physics, Faculty of Sci, University of Thamar , Thamar, Yemen,**
[4]**Department of Physics, College of Science and Arts, Najran University, Najran, Saudi Arabia**

*Corresponding author: a.alkelly@su.edu.ye

Abstract

Based on the mathematical framework of the partially coherent Gaussian Schell model vortex (PCGSMV) beam and the Huygens-Fresnel integral, we conducted a study to analyze the intensity distribution and depth of focus (DOF) of the PCGSMV beam as it propagates through a classical axicon. Our numerical results indicate the influence of factors such as the beam width, spatial degree of coherence, topological charge, and axicon base angle on the intensity distribution and DOF. In addition, we investigated the relationship between the beam spot size and propagation distance, as well as the effects of the spatial degree of coherence and propagation distance on the intensity profile. Our findings highlight the importance of the intensity values along the DOF for various applications, including the optical trapping and manipulation of micro-particles.

Article Info

Keywords:
partially coherent, Gaussian Schell model, vortex, dark hollow, lensacon, astigmatic aberration, depth of focus.

Article History:
Received: 23-Septemper-2024,
Revised: 30-Septemper-2024,
Accepted: 13-October-2024,
Available online: 31 October 2024.

1. INTRODUCTION

In recent years, partially coherent beams have exhibited unique optical properties and have demonstrated superiority in various applications, including optical communication, noise reduction in photography, laser nuclear fusion, and classical ghost interference [1–4]. Additionally, partially coherent beams have outperformed coherent beams in various applications, such as laser scanning, optical scattering, atom cooling, and particle trapping [5–8]. Partially coherent Gaussian Schell-model beams have been extensively studied both theoretically and experimentally, and their simple functional form makes them suitable for a variety of applications, including free-space optical communication, particle trapping, and optical scattering. Recently, vortex beams have been shown to possess specific topological charges, spiral wavefront structures, and ring shapes with zero central intensity. Owing to these characteristics, vortex beams have gained popularity 1owing to their variety of focal shapes, featuring unique attributes such as beam shaping, beam rotation, and applications in various fields, including the manipulation of particles, optical patterning, optical tweezers, non-linear optics, dark spots, and laser communication [9–12]. Additionally, the partially coherent Gaussian Schell-model vortex beam represents a typical type of vortex beam that has been extensively studied in various media, such as gradient index media, turbulent plasma atmosphere, free space, oceanic environments, and biological tissues [13–18]. Lian-zhou et al. studied the properties of a partially coherent vortex beam focused by an aperture lens [19]. Shukri et al. studied the intensity distribution of PCGSMV beam diffracted by axicon. Lensacon has gained interest because of its versatility and utility in producing various beam shapes with different focal lengths. Koronkevich et al. (1993) [20] described the first lens and axicon combi-

nation (lensacon) that formed a conical beam distribution instead of Bessel beam that formed by classical axicon. Lensacon is characterized by producing a high-quality focal ring that can be utilized in hole-drilling applications [21] and other applications, such as surgery for smoothing and ablating corneal tissue [22], and is used as a corrective element in the optical system of the human eye [23], laser structuring, micro-machining, optical trapping, optical capture and manipulation of micro-particles, sensors, and atom guidance [24–29]. The Qusailah et al. Studied the Intensity distribution of lensacon illuminated by partially coherent Gaussian Schell vortex beam [30]. Astigmatic aberration causes an optical system to exhibit different optical properties. The deformation of the beam structure emerging from the lensacon results from various beam transmission mechanisms through the optical system. Because of the significant difference between systems with and without astigmatic aberration in the optical wave propagation mechanism, it is of interest to investigate the propagation of a PCGSMV beam in a lensacon in presence of astigmatic aberration; to the best of our knowledge, this has not yet been explored. In despite there are wide studied to investigate the DOF and spot size of beams, such as apodization of the focusing system is used to extended DOF adaptive optics spectral domain optical coherence tomography [31], the extended depth of field microscope imaging system with the phase pupil mask [32], dynamic focal shift and extending depth of focus based on the masking of the illuminating beam and using an adjustable axicon [33], power phase apodization study on compensation defusing and chromatic aberration in the imaging system [34] and Freestyle 3D laser traps [35]. The DOF that shaped by axicon and perfect lensacon explored by [30, 36]. In this study, we developed a mathematical model to describe the propagation of a PCGSMV beam diffracted by a lensacon with astigmatic aberration and numerically investigated the effect of astigmatic aberration on the propagation of a PCGSMV beam through a lensacon and the spatial correlation length of the beam based on the Huygens-Fresnel integral. This study aimed to provide a comprehensive understanding of astigmatic aberration and its effect on the interaction between lensacons and beams. We hope that this study will lead to new exploration and innovative applications in scientific research.

2. MATH AND EQUATIONS

The initial field of the Gaussian vortex (GV) beam at the plane $z = 0$ in cylindrical coordinates can be written as [37]

$$u(\rho', z = 0) = \sqrt{G_0}\ \exp\left[i\ m\ \phi'\right]\ \exp\left[-\frac{\rho'^2}{w^2}\right], \quad (1)$$

where G_0 is the amplitude constant of the beam, $\rho' = \sqrt{x'^2 + y'^2}$, w is the waist width of the Gaussian part, ϕ' is the azimuthal angle, and m is the topological charge. The cross-spectral density (CSD) of the PCGSMV beam in the presence of the Schell-correlator at the source plane is defined as [38]

$$W_{in}(\boldsymbol{\rho_1'}, \boldsymbol{\rho_2'}, z = 0) = \left\langle u^*(\boldsymbol{\rho_1'}, z = 0) * u(\boldsymbol{\rho_2'}, z = 0)\right\rangle, \quad (2)$$

where $\boldsymbol{\rho_1'}$ and $\boldsymbol{\rho_2'}$ are two arbitrary points on the source plane. By considering the correlation function, which is expressed as $\eta(\boldsymbol{\rho_1'} - \boldsymbol{\rho_2'}) = \exp\left(-\frac{|\boldsymbol{\rho_1'} - \boldsymbol{\rho_2'}|^2}{2\sigma^2}\right)$ where $\boldsymbol{\rho_1'} = (\rho_1', \phi_1')$, $\boldsymbol{\rho_2'} = (\rho_2', \phi_2')$ and σ are the spatial correlations of coherence length. We can rewrite Eq. (2) as follows [39]

$$\begin{aligned} W_{in}(\boldsymbol{\rho_1'}, \boldsymbol{\rho_2'}, z = 0) =& G_0\ \exp\left[-({\rho_1'}^2 + {\rho_2'}^2)\left(\frac{1}{w^2} + \frac{1}{2\sigma^2}\right)\right] \\ &\times \exp\left[i\ m\ (\phi_2' - \phi_1')\right] \\ &\times \exp\left[\frac{\rho_1'\ \rho_2' \cos(\phi_2' - \phi_1')}{\sigma^2}\right]. \end{aligned} \quad (3)$$

The diffracted field $u(\boldsymbol{\rho}, z)$ at z distance from the source plan of the PCGSMV beam lensacon in presence of astigmatic aberration in the Huygens-Fresnel (H-F) integral approach is written as [40]:

$$\begin{aligned} u(\boldsymbol{\rho}, \phi, z) = \left(\frac{-i\ k}{2\ \pi\ z}\right) \exp\left[i\ k\ z\right] \int_0^a \int_0^{2\pi} A(\boldsymbol{\rho'}) \\ \times \exp\left[\frac{i\ k}{2z}\ |\boldsymbol{\rho} - \boldsymbol{\rho'}|^2\right] \rho' d\rho' d\phi', \end{aligned} \quad (4)$$

where $k = \frac{2\ \pi}{\lambda}$ and k is the wave number with wavelength λ and $A(\boldsymbol{\rho'})$ defined as

$$A(\boldsymbol{\rho'}) = u(\boldsymbol{\rho'}, z = 0) A_{axicon}(\boldsymbol{\rho'}) A_{lens}(\boldsymbol{\rho'}), \quad (5)$$

where $u(\boldsymbol{\rho'}, z = 0)$ is the initial field of the PCGSMV beam, $A_{axicon}(\boldsymbol{\rho'})$ is the axicon transmission function defined as [36]

$$A_{axicon}(\boldsymbol{\rho'}) = \exp\left[-i\ k\ \rho'\ (n - 1)\ \alpha\right], \quad (6)$$

where α is the axicon base angle given by the beam deviation angle for the propagation axis, which is defined as [28] $\theta = \arcsin(n \sin(\alpha)) - \alpha$, n is the refractive index of the axicon, and $A_{lens}(\boldsymbol{\rho'})$ is the transmission function of the lens, which can be obtained as

$$A_{lens}(\boldsymbol{\rho'}) = \exp\left[-i\ k\ {\rho'}^2\left(\frac{\mu + 1}{4f} - \frac{(\mu - 1)\ \cos 2\phi'}{4\ f}\right)\right], \quad (7)$$

where f denotes the focal length and μ is the astigmatic coefficient [28]. By substituting Eq. (1), Eq. (6), and Eq. (7) into Eq. (5), and substituting Eq. (5) into Eq. (4), we can evaluate the field diffraction from the lensacon plane with radial coordinates $(\rho_1', \phi_1', z = 0)$ to the image plane

with radial coordinates (ρ_1, ϕ_1, z) at z position as follows

$$u(\boldsymbol{\rho}_1, \phi_1, z) = \frac{-i\,k}{2\,\pi\,z}\sqrt{G_0}\exp\left[i\,k\,\left(z+\frac{\rho_1^2}{2z}\right)\right]\int_0^a\int_0^{2\pi}\rho_1' \times \exp\left[i\,m\,\phi_1'\right] \times \exp\left[i\,k\,\left(\frac{\mu+1}{4\,f}-\frac{1}{2\,z}\right)\left(\rho_1'^2-\rho_2'^2\right)\right] \times \exp\left[-\frac{\rho_1'^2}{w^2}\right]\exp\left[-i\,k\,\rho_1'\,((n-1)\,\alpha)\right] \times \exp\left[\frac{-i\,k\,\rho_1\rho_1'\cos(\phi_1-\phi_1')}{z}\right] \times \exp\left[\frac{i\,k\,(\mu-1)\rho_1'^2\,cos(2\phi_1')}{4\,f}\right]d\rho_1' d\phi_1'. \tag{8}$$

For a PCGSMV wave field, the statistical characteristics and correlation properties of the incident stationary wave field must be described by the following formula

$$W_{out}(\boldsymbol{\rho}_1', \boldsymbol{\rho}_2', z) = \left\langle u^*(\rho_1', \phi_1', z=0) * u(\rho_2', \phi_2', z=0)\right\rangle. \tag{9}$$

Substituting Eq. (8) into Eq. (9), the CSD of the PCGSMV beam can be expressed as

$$W_{out}(\boldsymbol{\rho}_1, \boldsymbol{\rho}_2, z) = \left(\frac{k}{2\pi\,z}\right)^2 G_0\,\exp\left[\frac{i\,k\,(\rho_2^2-\rho_1^2)}{2z}\right] \times \int_0^a\int_0^a\int_0^{2\pi}\int_0^{2\pi}(\rho_1'\,\rho_2') \times \exp\left[-(\rho_1'^2+\rho_2'^2)\left(\frac{1}{w^2}+\frac{1}{2\sigma^2}\right)\right] \times \exp\left[i\,m\,(\phi_2'-\phi_1')\right] \times \exp\left[\frac{\rho_1'\,\rho_2'\cos(\phi_2'-\phi_1')}{\sigma^2}\right] \times \exp\left[i\,k\,(\rho_1'-\rho_2')\,((n-1)\,\alpha)\right] \times \exp\left[i\,k\,\left(\frac{\mu+1}{4\,f}-\frac{1}{2\,z}\right)\left(\rho_1'^2-\rho_2'^2\right)\right] \times \exp\left[\frac{-i\,k\,\rho_2\,\rho_2'\cos(\phi_2-\phi_2')}{z}\right] \times \exp\left[\frac{i\,k\,\rho_1\,\rho_1'\cos(\phi_1-\phi_1')}{z}\right] \times \exp\left[\frac{-i\,k\,(\mu-1)\,\rho_1'^2\cos(2\phi_1')}{4f}\right] \times \exp\left[\frac{i\,k\,(\mu-1)\,\rho_2'^2\cos(2\phi_2')}{4f}\right] \times d\rho_1' d\rho_2' d\phi_1' d\phi_2', \tag{10}$$

using the Jacobi-Anger expansion that is given by [41]

$$\exp\left[\frac{i\,k\,\rho_1'\,\rho_1\,\cos(\phi_1-\phi_1')}{z}\right] = \sum_{l=-\infty}^{\infty}(i)^l J_l\left[\frac{k\,\rho_1'\,\rho_1}{z}\right] \times \exp\left[\,i\,l\,(\phi_1-\phi_1')\right], \tag{11}$$

where $J_l(.)$ is the first type of Bessel function of order l and

$$\exp\left[\frac{i\,k\,(\mu-1)\,\rho_1'^2\cos 2\phi_1'}{4f}\right] = \sum_{q=-\infty}^{\infty}(i)^q \times J_q\left[\frac{k\,(\mu-1)\,\rho_1'^2}{4\,f}\right]\times\exp\left[2\,i\,q\phi_1'\right], \tag{12}$$

where $J_q(.)$ is the first type of Bessel function of order q. By substituting Eq. (12) and Eq. (11) into Eq. (10), we rewrite Eq. (10) as

$$W_{out}(\boldsymbol{\rho}_1, \boldsymbol{\rho}_2, z) = \left(\frac{k}{2\,\pi\,z}\right)^2 G_0\exp\left[\frac{-i\,k\,(\rho_1^2-\rho_2^2)}{2z}\right] \times \sum_{q=-\infty}^{\infty}\sum_{l=-\infty}^{\infty}\int_0^a\int_0^a\int_0^{2\pi}\int_0^{2\pi}(\rho_1'\,\rho_2') \times \exp\left[-(\rho_1'^2+\rho_2'^2)\left(\frac{1}{w^2}+\frac{1}{2\sigma^2}\right)\right] \times \exp\left[\frac{\rho_1'\,\rho_2'\cos(\phi_2'-\phi_1')}{\sigma^2}\right] \times \exp\left[i\,k\,(\rho_1'-\rho_2')((n-1)\,\alpha)\right] \times \exp\left[i\,k\,\left(\frac{\mu+1}{4\,f}-\frac{1}{2\,z}\right)\left(\rho_1'^2-\rho_2'^2\right)\right] \times J_l\left[\frac{k\,\rho_1\,\rho_1'}{z}\right]J_l\left[\frac{k\,\rho_2\rho_2'}{z}\right] \times J_q\left[\frac{k\,(\mu-1)\,\rho_1'^2}{4\,f}\right]\exp\left[i\,m\,(\phi_2'-\phi_1')\right] \times J_q\left[\frac{k\,(\mu-1)\,\rho_2'^2}{4\,f}\right]\exp\left[-i\,l\,(\phi_2-\phi_2')\right] \times \exp\left[2\,i\,q\,(\phi_2'-\phi_1')\right]\exp\left[i\,l(\phi_1-\phi_1')\right] \times d\rho_1'\,d\rho_2'\,d\phi_1'\,d\phi_2'. \tag{13}$$

Letting $\rho_1 = \rho_2 = \rho$, and $\phi_1 = \phi_2 = \phi$, we rewrite Eq.(13) as

$$W_{out}(\rho, z) = \left(\frac{k}{2\pi z}\right)^2 G_0\sum_{q=-\infty}^{\infty}\sum_{l=-\infty}^{\infty}\int_0^a\int_0^a\int_0^{2\pi}\int_0^{2\pi} \times(\rho_1'\,\rho_2')\exp\left[-(\rho_1'^2+\rho_2'^2)\left(\frac{1}{w^2}+\frac{1}{2\sigma^2}\right)\right] \times \exp\left[i\,(l+m+2q)(\phi_2'-\phi_1')\right] \times \exp\left[\frac{\rho_1'\,\rho_2'\cos(\phi_2'-\phi_1')}{\sigma^2}\right] \times \exp\left[i\,k\,(\rho_1'-\rho_2')((n-1)\,\alpha)\right] \times \exp\left[i\,k\,\left(\frac{\mu+1}{4\,f}-\frac{1}{2\,z}\right)\left(\rho_1'^2-\rho_2'^2\right)\right] \times J_l\left[\frac{k\,\rho\,\rho_1'}{z}\right]J_l\left[\frac{k\,\rho\,\rho_2'}{z}\right] \times J_q\left[\frac{k(\mu-1)\rho_1'^2}{4\,f}\right]J_q\left[\frac{k\,(\mu-1)\,\rho_2'^2}{4\,f}\right] \times d\rho_1'\,d\rho_2'\,d\phi_1'\,d\phi_2'. \tag{14}$$

Using the relation

$$I_{(m+l+2q)}\left[\frac{\rho_1'\,\rho_2'}{\sigma^2}\right]=\frac{1}{4\,\pi^2}\int_0^{2\pi}\int_0^{2\pi}\times\exp\left[\frac{\rho_1'\,\rho_2'\cos(\phi_2'-\phi_1')}{\sigma^2}\right]\times\exp\left[i\,(m+l+2q)(\phi_2'-\phi_1')\right]d\phi_1'd\phi_2', \tag{15}$$

where I_{m+l+2q} is the modified Bessel function of the first kind and order $(m+l+2q)$ and by substituting Eq. (15) into Eq. (14), we can rewrite Eq. (13) as

$$\begin{aligned}W_{out}(\rho,z)=&\left(\frac{k}{z}\right)^2 G_0\sum_{q=-\infty}^{\infty}\sum_{l=-\infty}^{\infty}\int_0^a\int_0^a(\rho_1'\,\rho_2')\\&\times\exp\left[-(\rho_1'^2+\rho_2'^2)\left(\frac{1}{w^2}+\frac{1}{2\sigma^2}\right)\right]\\&\times\exp\left[i\,k\,(\rho_1'-\rho_2')\,((n-1)\,\alpha)\right]\\&\times\exp\left[i\,k\,\left(\frac{\mu+1}{4\,f}-\frac{1}{2\,z}\right)\left(\rho_1'^2-\rho_2'^2\right)\right]\\&\times J_l\left[\frac{k\,\rho\,\rho_1'}{z}\right]J_l\left[\frac{k\,\rho\,\rho_2'}{z}\right]I_{(m+l+2q)}\left[\frac{\rho_1'\,\rho_2'}{\sigma^2}\right]\\&\times J_q\left[\frac{k\,(\mu-1)\,\rho_1'^2}{4f}\right]J_q\left[\frac{k\,(\mu-1)\,\rho_2'^2}{4f}\right]\\&\times d\rho_1'\,d\rho_2'.\end{aligned} \tag{16}$$

To solve Eq. (16), we use the stationary phase (SP) method [30]. The total phase function of the lensacon in presence of astigmatic aberration can be obtained as

$$F(\rho')=((n-1)\,\alpha)\;\rho'+\left(\frac{\mu+1}{4f}-\frac{1}{2z}\right)\rho'^2. \tag{17}$$

Applying the stationary phase method, we can express the stationary point as

$$\rho_{Sp}'=\frac{-(n-1)\,\alpha}{\frac{\mu+1}{2f}-\frac{1}{z}}. \tag{18}$$

Substituting Eq. (18) into Eq. (16), we can obtain the numerical model of the CSD of the PCGSMV beam propagation through the lensacon in presence of astigmatic aberration as

$$\begin{aligned}W_{out}(\rho,z)=&\,G_0\left(\frac{2\,\pi\,k}{z^2\left(\frac{\mu+1}{2\,f}-\frac{1}{z}\right)}\right)\left(\frac{(n-1)\,\alpha}{(\frac{\mu+1}{2f}-\frac{1}{z})}\right)^2\\&\times\exp\left[-\left(\frac{(n-1)\,\alpha}{(\frac{\mu+1}{2\,f}-\frac{1}{z})}\right)^2(\frac{2}{w^2}+\frac{1}{\sigma^2})\right]\\&\times\sum_{l=-\infty}^{\infty}\sum_{q=-\infty}^{\infty}I_{(m+l+2q)}\left[\frac{(\frac{(n-1)\,\alpha}{(\frac{\mu+1}{2\,f}-\frac{1}{z})})^2}{\sigma^2}\right]\\&\times J_l\left[\frac{k\,\rho\,(\frac{(n-1)\,\alpha}{(\frac{\mu+1}{2\,f}-\frac{1}{z})})}{z}\right]^2\times J_q\left[\frac{k\,(\mu-1)\,(\frac{(n-1)\,\alpha}{(\frac{\mu+1}{2\,f}-\frac{1}{z})})^2}{4\,f}\right]^2\end{aligned} \tag{19}$$

3. DEPTH OF FOCUS

In lensacon, the DOF is [30]

$$DOF=\frac{w}{(n-1)\,\alpha+\frac{w}{f}}. \tag{20}$$

Suppose that for a lens in presence of astigmatic aberration, we replace the term $\frac{w}{f}$ in Eq. (20) by $\frac{w\,(\mu+1)}{2f}$. Notably, PCGSMV beams exhibit an effective beam width w_{eff} [42], which can be expressed as follows

$$w_{eff}=\left(\frac{1}{(2w)^4}+\frac{1}{(2w)^2\sigma^2}\right)^{-\frac{1}{4}}. \tag{21}$$

Replacing w with w_{eff} in Eq. (20), the DOF of the PCGSMV beam can be obtained as

$$DOF=\frac{\left(\frac{1}{(2w)^4}+\frac{1}{(2w)^2\sigma^2}\right)^{-\frac{1}{4}}}{(n-1)\,\alpha+\frac{(\mu+1)\left(\frac{1}{(2w)^4}+\frac{1}{(2w)^2\,\sigma^2}\right)^{\frac{-1}{4}}}{2f}}. \tag{22}$$

4. RESULT AND DISSECTION

Numerical calculations were performed using Mathematica 10. Based on Eq. (19), the parameters of the PCGSMV beam and lensacon system in the numerical calculation are f = 100 mm, λ = 632.7 nm, n = 1.5, m = 1, and G_0 = 1 $watt/mm^2$. Fig. 1 shows the axial inten-

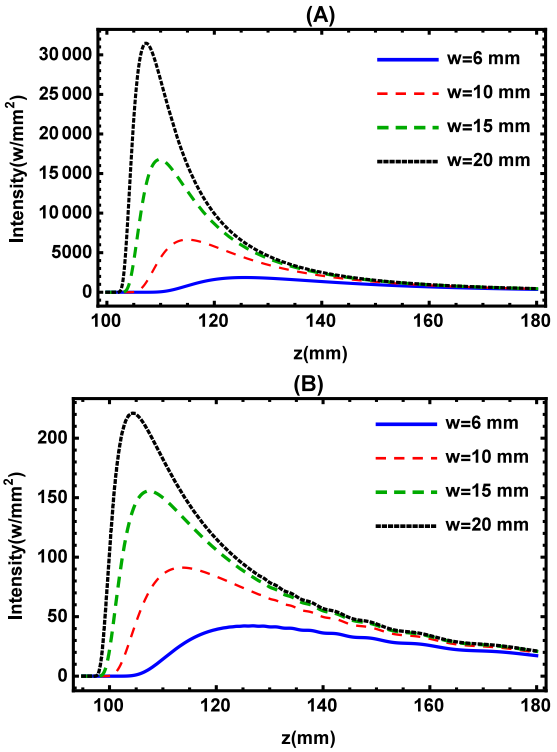

Figure 1. Axial intensity distribution of the PCGSMV beam focused by the lensacon without aberration (A) and in presence of astigmatic aberration (B) for axicon base angle $\alpha = 0.02$ rad, beam width $w = 6$ mm, astigmatic coefficient $\mu = 1.1$ and spatial correlation of coherence length $\sigma = 2$ mm.

sity distribution of the PCGSMV beam at various beam widths for the lensacon, comparing Fig. 1 (A) and (B). The observed trend indicates a gradual increase in the intensity distribution with the beam width w owing to the energy carried by the beam width, and noticeable displacement of the intensity maximum towards smaller z values as the beam width w increases in both Figs. 1 (A) and (B). Additionally, the intensity in Fig. 1 (A) surpasses that in Fig. 1 (B) because of the influence of astigmatic aberration. Specifically, for a beam width of $w = 20$ mm, the intensity produced by the lensacon at $z = 110$ mm was 150 times greater than that generated by the lensacon in presence of astigmatic aberration. The contour plot in Fig. 2 illustrates the radial intensity distribution of the PCGSMV beam diffracted by the lensacon in presence of astigmatic aberration, considering various values of σ at different propagation distances. In general, the incorporation of a lens in presence of astigmatic aberration into an axicon system enhances the degree of freedom of the system. This modification is expected to affect the behavior of the beam during propagation, as indicated by Eq. (19). Anticipated changes involve a gradual transition from a flat-topped profile into half dark hollow with propagating direction. This behavior is demonstrated when the spatial coherence is low ($\sigma = 2$ mm), indicating the disappearance of the dark spot of the vortex effect under conditions of low coherence. Conversely, for higher values of σ, the profile of transforms from a flat-topped with increasing propagation distance, ultimately transitioning into a wide-diameter dark hollow spot at a far distance owing to the effect of astigmatic aberration and vortex. In addition, oscillations were observed in the flat-topped profile affected by the astigmatic coefficient, spatial coherence, and propagation distance, and the amplitude of these oscillations increased with both spatial coherence σ and astigmatic aberration coefficient. In this context, the impact of the vortex profile became more appearance as σ increase. Fig. 3 depicts the radial intensity distribution of the beam concentrated by the lensacon in presence of astigmatic aberration for various values of the astigmatic coefficient at different propagation distances. Notably, the observed trend reveals a reduction in intensity corresponding to an increase in the astigmatic coefficient. Additionally, we observed a gradual transformation of the flat-topped profile to dark hollow profile as the propagation distance increased. Remarkably, at long propagation distances, a notable shift in the beam profile occurs, manifesting as a half dark hollow with a wide-diameter dark spot. This transformation can be attributed to astigmatic aberrations. This analysis contributes to our understanding of the spatial dynamics of astigmatic aberrations in beam properties focused by a lensacon.

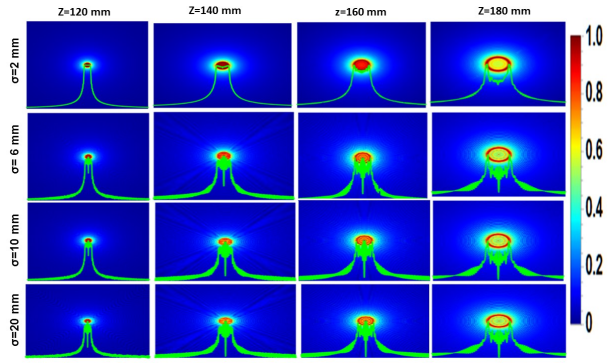

Figure 2. The contour plots of the intensity distribution of the PCGSMV formed by lensacon in presence of astigmatic aberration coefficient $\mu = 1.1$ and axicon base angle $\alpha = 0.02$ rad at several propagation distances z, $m = 1$, $w = 6$ mm, for different σ.

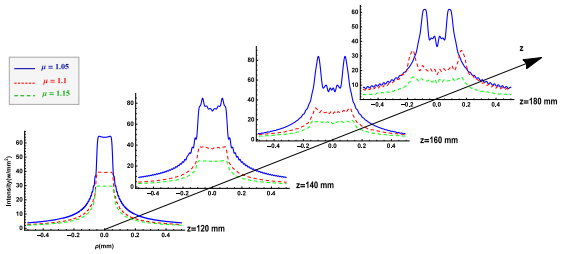

Figure 3. Radial intensity distribution of the PCGSMV focused by lensacon in presence of astigmatic aberration for propagation distance z, $w = 6$ mm, $\sigma = 2$ mm, $m = 1$, and base angle $\alpha = 0.02$ rad for different astigmatic aberrations μ.

Fig. 4 depicts the relationship between the intensity, σ, and α at various propagation distances. Fig. 4 (A) highlights that at lower σ values, the constant of the intensity before σ_{drop} owing to the effect of astigmatic aberration. σ_{drop} is defined as the point at which the intensity starts decreasing as a result of the vortex effect. Subsequently, there is a gradual reduction in intensity as σ increases, influenced by the vortex, and a decrease in intensity with an increase in propagation distance, accompanied by a shift in σ_{drop} towards smaller σ values with propagation. Fig. 4 (B) illustrates the influence of the axicon base angle on the intensity. The intensity increased with the axicon base angle until it reaches α_{max}, followed by a decline with α. Geometrically, the decreases in intensity after α_{max} can be attributed to the internal reflection by the axicon. Moreover, there is an observed shift in α_{max} towards a larger α with an increase in the propagation distance. In addition,it can be observed that the oscillation in all curves owing to the effect of astigmatic aberration.

Fig. 5 illustrates the effect of the astigmatic coefficient on the intensity distribution. As depicted in Fig. 5 (A) and (B), there is a gradual reduction in intensity with an increase in μ, which is attributed to the energy dissipation resulting from scattering induced by astigmatic aberra-

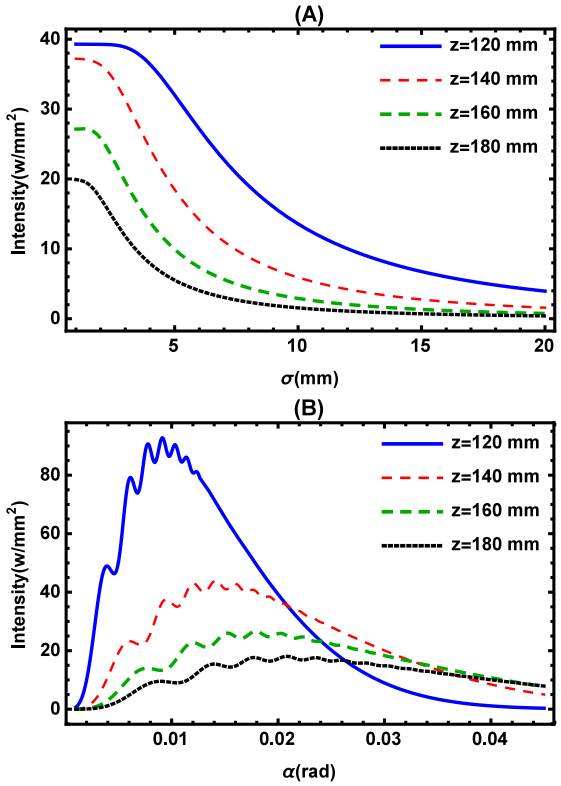

Figure 4. The intensity distribution of the PCGSMV beam focused by lensacon in presence of astigmatic aberration as a function of (A) spatial degree of coherence σ at various z, $w = 6$ mm, $\alpha = 0.02$ rad, and $\mu = 1.1$ and (B) axicon base angle α, $m = 1$ and $\sigma = 2$ mm.

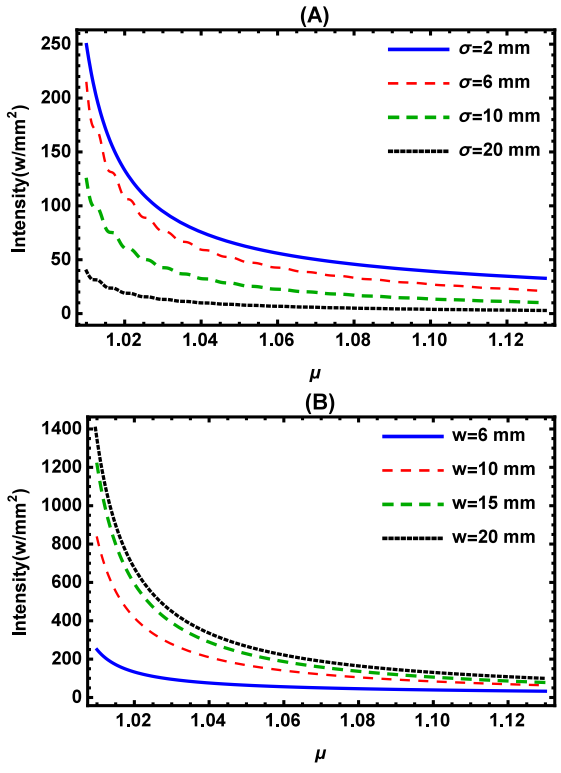

Figure 5. Relation Intensity distribution of the PCGSMV beam as a function of astigmatic coefficient at $z = 120$ mm, $\alpha = 0.02$ rad for spatial correlation of the coherence length (A) and $w = 6$ mm, and the beam width w (B), and σ=2 mm.

tion. The astigmatism directs the beam to converge at distinct points along the paraxial axis. The probability of beam convergence on the optical axis diminishes with the increasing astigmatism coefficient. Furthermore, in Fig. 5 (A), it becomes apparent that the intensity improves at a lower σ, transitioning from the blue curve to the red curve. Conversely, the intensity decreases from the red curve to the black curve as σ increases. Fig. 6

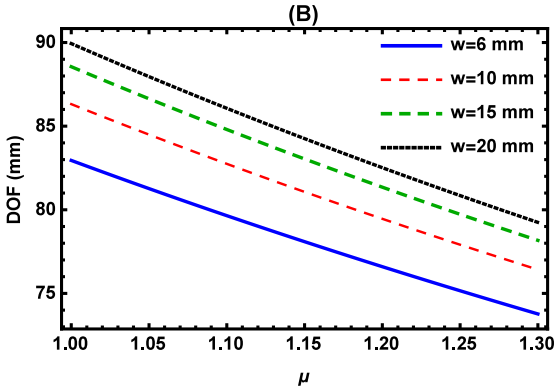

Figure 6. (A) The depth of focus (DOF) as a function of spatial degree of coherence length σ for different values of w and (B) DOF as a function of μ for different w, $\sigma = 2$ mm, $\alpha = 0.02$ rad. All curves obtained by the Eq. (22).

shows the effect of the beam width and spatial degree of coherence on the DOF. It can be observed that the DOF increased as the beam width increase. In Fig. 6 (A), it is observed that the DOF rapidly increases with σ for low σ values, but the relationship between the DOF and σ becomes non-linear with increase σ. Furthermore, It can be observed from Fig. 6 (A) increase the DOF with increase w . Fig. 6 (B) illustrates the relationship between depth and the astigmatic coefficient. It is noticeable that there is a linear decrease in the depth of focus an the increase in the astigmatic coefficient. It can be seen from this Fig. that the DOF is 79 mm for $\mu = 1.1$, $w = 6$ mm and $\sigma = 2$ mm,

5. CONCLUSION

Our study focuses on examining the behavior of a PCGSMV beam as it passes through an aberrated astigmatic lensacon. By considering of various parameters and configurations, we obtain a comprehensive understanding of how astigmatic aberrations influence the performance of optical systems. A formula was developed to depict the relationship between the depth of the focus and the astigmatic aberration coefficient. The numerical results provide insights into the influence of astigmatic aberration on the beam structure, intensity distribution, and depth of focus. In the presence of astigmatism, we noted a reduction in the intensity and enlargement of the spot size. With an increase in the propagation distance, the beam profile gradually transitioned a flat-topped pro-

file to dark hollow profile, particularly for low values of the spatial degree of coherence length. Our numerical findings revealed a progressive shift in the profile from flat-topped to a dark hollow profile, as the spatial degree of coherence increased. For extensive propagation distances, our results demonstrated a wide dark hollow with oscillations, attributed to the effect of astigmatic aberration. Furthermore, the results emphasized the influence of the beam width, spatial degree of coherence length, axicon base angle, and astigmatic coefficient on the intensity distribution and depth of focus.

REFERENCES

[1] X. Wang, L. Wang, and S. Zhao, "Propagation properties of an off-axis hollow gaussian-schell model vortex beam in anisotropic oceanic turbulence," J. Mar. Sci. Eng. **9**, 1139 (2021).

[2] A. Beléndez, L. Carretero, and A. Fimia, "The use of partially coherent light to reduce the efficiency of silver halide noise gratings," Opt. Commun. **98**, 236–240 (1993).

[3] Y. Kato, K. Mima, N. Miyanaga, *et al.*, "Random phasing of high-power lasers for uniform target acceleration and plasma-instability suppression," Phys. Rev. Lett. **53**, 1057–1060 (1984).

[4] Y. Cai and S.-Y. Zhu, "Ghost imaging with incoherent and partially coherent light radiation," Phys. Rev. E **71**, 056607 (2005).

[5] C. Ding, Y. Cai, O. Korotkova, *et al.*, "Scattering-induced changes in the temporal coherence length and the pulse duration of a partially coherent plane-wave pulse," Opt. letters **36**, 517–519 (2011).

[6] T. van Dijk, D. G. Fischer, T. D. Visser, and E. Wolf, "Effects of spatial coherence on the angular distribution of radiant intensity generated by scattering on a sphere," Phys. review letters **104**, 173902 (2010).

[7] J.-F. Zhang, Z.-Y. Wang, B. Cheng, *et al.*, "Atom cooling by partially spatially coherent lasers," Phys. Rev. A **88**, 023416 (2013).

[8] C. Zhao, Y. Cai, X. Lu, and H. T. Eyyuboğlu, "Radiation force of coherent and partially coherent flat-topped beams on a rayleigh particle," Opt. express **17**, 1753–1765 (2009).

[9] C. Zhao and Y. Cai, "Trapping two types of particles using a focused partially coherent elegant laguerre–gaussian beam," Opt. Lett. **36**, 2251–2253 (2011).

[10] S. N. Khonina and S. A. Degtyarev, "Analysis of the formation of a longitudinally polarized optical needle by a lens and axicon under tightly focused conditions," J. Opt. Technol. **83**, 197–205 (2016).

[11] J. Xu, T. Geng, X. Gao, and S. Zhuang, "Generation of a dark spot beyond the diffraction limit with a radially polarized vortex beam," J. Opt. Soc. Am. A **34**, 2165–2169 (2017).

[12] I. G. Loqman, A. Alkelly, and H. T. Al-Ahsab, "Propagation of azimuthally polarized bessel-gaussian beam through helical axicon," Available at SSRN 4029007 (2022).

[13] M. S. Qusailah, A. A. Alkelly, W. A. Al-Bahry *et al.*, "The propagation properties of a lorentz–gauss vortex beam in a gradient-index medium," Int. J. Opt. **2023** (2023).

[14] A. A. Alkelly, M. H. Khaled, and L. F. Hassan, "Angular width and beam quality of a partially coherent standard laguerre–gaussian vortex beam in turbulent plasma," JOSA A **41**, 45–53 (2024).

[15] H. AL-Nadary, A. A. Alkelly, M. Khaled, and L. F. Hassan, "The effective beam width of a partially coherent rectangular multi-gaussian schell-model vortex beam propagating in a turbulent plasma," Sana'a Univ. J. Appl. Sci. Technol. **1** (2023).

[16] S. Chang, Y. Song, Y. Dong, and K. Dong, "Spreading properties of a multi-gaussian schell-model vortex beam in slanted atmospheric turbulence," Opt. Appl. **50** (2020).

[17] X. Ma, G. Wang, H. Zhong, *et al.*, "The off-axis multi-gaussian schell-model hollow vortex beams propagation in free space and turbulent ocean," Optik **228**, 166180 (2021).

[18] M. Duan, Y. Tian, and J. Li, "Propagation of gaussian schell-model vortex beams in biological tissues," Opt. Appl. **49**, 203–215 (2019).

[19] R. Lian-Zhou and P. Ji-Xiong, "Focusing of partially coherent vortex beams by an aperture lens," Chin. Phys. Lett. **24**, 1252 (2007).

[20] V. Koronkevich, I. Mikhaltsova, E. Churin, and Y. I. Yurlov, "Lensacon," Appl. Opt. **34**, 5761–5772 (1995).

[21] M. Duocastella and C. B. Arnold, "Bessel and annular beams for materials processing," Laser & Photonics Rev. **6**, 607–621 (2012).

[22] O. Ren and R. Birngruber, "Axicon: a new laser beam delivery system for corneal surgery," IEEE journal quantum electronics **26**, 2305–2308 (1990).

[23] G. Lenkova, "Spatial-energy characteristics of the focal areas of bifocal diffractive-refractive intraocular lenses," Optoelectron. Instrum. Data Process. **53**, 68–76 (2017).

[24] I. Manek, Y. B. Ovchinnikov, and R. Grimm, "Generation of a hollow laser beam for atom trapping using an axicon," Opt. communications **147**, 67–70 (1998).

[25] M. Chen, M. Mazilu, Y. Arita, *et al.*, "Dynamics of microparticles trapped in a perfect vortex beam," Opt. letters **38**, 4919–4922 (2013).

[26] S. Syubaev, A. Zhizhchenko, O. Vitrik, *et al.*, "Chirality of laser-printed plasmonic nanoneedles tunable by tailoring spiral-shape pulses," Appl. Surf. Sci. **470**, 526–534 (2019).

[27] A. Ashkin, "Acceleration and trapping of particles by radiation pressure," Phys. review letters **24**, 156 (1970).

[28] S. N. Khonina, N. L. Kazanskiy, P. A. Khorin, and M. A. Butt, "Modern types of axicons: New functions and applications," Sensors **21**, 6690 (2021).

[29] S. Castillo, "Axicons in action: Unique wavefront sensing for adaptive optics," Optik & Photonik **11**, 36–39 (2016).

[30] M. S. Qusailah, A. A. Alkelly, H. O. Al-Nadary, *et al.*, "Depth of focus and intensity distribution of a lensacon illuminated by a partially coherent gaussian schell vortex beam," Appl. Opt. **63**, 3138–3147 (2024).

[31] K. Sasaki, K. Kurokawa, S. Makita, and Y. Yasuno, "Extended depth of focus adaptive optics spectral domain optical coherence tomography," Biomed. optics express **3**, 2353–2370 (2012).

[32] Q. Lyu, Z. Zhai, M. Sharp, and P. French, "The extended depth of field microscope imaging system with the phase pupil mask," in *Selected Papers of the Photoelectronic Technology Committee Conferences held June–July 2015,* vol. 9795 (SPIE, 2015), pp. 426–431.

[33] S. N. Khonina, A. V. Ustinov, and A. P. Porfirev, "Dynamic focal shift and extending depth of focus based on the masking of the illuminating beam and using an adjustable axicon," JOSA A **36**, 1039–1047 (2019).

[34] S. N. Khonina, S. G. Volotovskiy, A. P. Dzyuba, *et al.*, "Power phase apodization study on compensation defocusing and chromatic aberration in the imaging system," Electronics **10**, 1327 (2021).

[35] J. A. Rodrigo and T. Alieva, "Freestyle 3d laser traps: tools for studying light-driven particle dynamics and beyond," Optica **2**, 812–815 (2015).

[36] S. A. M. Kaid, H. O. Al-Nadary, M. S. Qusailah, *et al.*, "Intensity distribution of the partially coherent gaussian schell vortex beam diffracted by classical axicon," jast **2**, 197–204 (May 2024).

[37] J. Zeng, R. Lin, X. Liu, *et al.*, "Review on partially coherent vortex beams," Front. Optoelectron. **12**, 229–248 (2019).

[38] M. Tang and D. Zhao, "Propagation of multi-gaussian schell-model vortex beams in isotropic random media," Opt. express **23**, 32766–32776 (2015).

[39] X. Liu, L. Liu, Y. Chen, and Y. Cai, "Partially coherent vortex beam: from theory to experiment," Vortex Dyn. Opt. Vortices pp. 275–296 (2017).

[40] M. Born *et al.*, "E. wolf principles of optics," Pergamon Press **6**, 36–111 (1980).

[41] G. B. Arfken, H. J. Weber, and F. E. Harris, *Mathematical methods for physicists: a comprehensive guide* (Academic press, 2011).

[42] J. Pu, "Beam quality changes of gaussian schell-model beams propagating through axicons," Opt. quantum electronics **30**, 265–270 (1998).